Magnetic and Electric Hotspots with Silicon Nanodimers

Reuben M. Bakker[1], Dmitry Permyakov[2], Ye Feng Yu[1], Dmitry Markovich[2], Ramón Paniagua-Domínguez[1], Leonard Gonzaga[1], Anton Samusev[2], Yuri Kivshar[2,3], Boris Luk'yanchuk[1], Arseniy I. Kuznetsov[1‡]*

1 Data Storage Institute, A*STAR, 5 Engineering Drive 1, 117608, Singapore

2 ITMO University, St. Petersburg, 197101, Russia

3 Nonlinear Physics Centre, Australian National University ACT 0200, Australia

* Reuben_Bakker@dsi.a-star.edu.sg

‡ Arseniy_K@dsi.a-star.edu.sg

ABSTRACT

The study of the resonant behavior of silicon nanostructures provides a new route for achieving efficient control of both electric and magnetic components of light. We demonstrate experimentally and numerically that enhancement of localized electric and magnetic fields can be achieved in a silicon nanodimer. For the first time, we experimentally observe hotspots of the magnetic field, at visible wavelengths for light polarized across the nanodimer's primary axis, using near-field scanning optical microscopy.

KEYWORDS. Nanoantenna, Silicon nanoparticle, Optically-induced magnetic resonances

Nanostructured dielectric materials with a high value of the refractive index have recently risen to prominence in the nanophotonics toolkit for control of light in the near-field [1-21]. They offer a novel way to directly engineer a magnetic field response at optical frequencies in addition to the electric field response in plasmonic structures. The basic building block – *a single dielectric spherical nanoparticle* – was shown to exhibit both electric and magnetic dipole resonances [1-10]. The magnetic resonance, recently experimentally demonstrated at visible frequencies in silicon (Si) [7-9] and gallium arsenide [10] nanoparticles, originates from circular displacement currents driven by an incident electric field, inducing a magnetic dipole moment perpendicular to the incident electric field. Similar to the case of plasmonic nanoparticles with electric dipoles, the induced magnetic dipole can be used to create more complex all-dielectric structures such as nanoantennas, metasurfaces and metamaterials [11-16]. Compared to metallic nanostructures employed in plasmonics, the near-fields in dielectric nanostructures immediately adjacent to the particles are less intense but can have larger far-field scattering cross sections [17]. Dielectric nanoparticles can reduce quenching and provide higher quantum efficiency of localized emitters than plasmonic structures which can be important for engineering emission at the subwavelength scale [17]. In addition to a single nanoparticle, *a nanodimer structure* should offer not only further tunability and engineering capabilities of the enhanced electric and magnetic fields but it should also reveal the physics of hotspots and near-field distributions known to be very important for nanoparticle oligomers with Fano-type resonances and strong inter-particle interactions [18, 19]. Dimer structures made of high-refractive-index materials have recently been studied through numerical calculations [17, 20-22] and also in experiments at microwave frequencies [23].

This letter reports the first experimental demonstration of both electric and magnetic hotspots of an isolated silicon nanodimer in the visible spectral range. Experimental data sets are obtained by using near-field scanning optical microscopy (NSOM), and they are compared with finite-difference time-domain (FDTD) simulations and multipole decomposition.

For the case of the high-index dielectric nanodimer when magnetic dipoles couple with each other, enhanced near-fields are expected, in analogy with the case of electric dipoles. The response of a nanodimer can be studied for two basic configurations: light polarized parallel to the dimer axis (X-polarized light) and light polarized perpendicular to the dimer axis (Y-polarized light), as illustrated in Figure 1. The physics of a plasmonic (metallic) dimer is well known. It produces a coupled resonance and subsequent electric field hotspot for incident light polarized along its primary axis but does not exhibit strong coupling for light orthogonal to its axis [17]. The dielectric nanodimer should exhibit coupled resonances for incident light polarized both along and orthogonal to its primary axis. As illustrated in Figure 1, for X-polarized light, the dielectric dimer exhibits coupling of the induced electric dipoles while for Y-polarized light there is coupling between the magnetic dipoles.

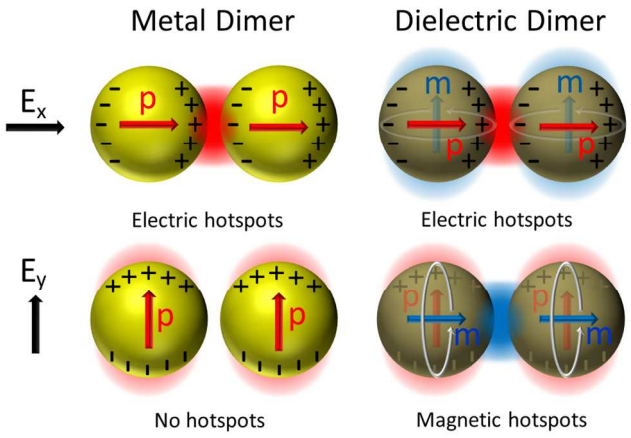

Figure 1. Comparison of metallic (plasmonic) and dielectric nanodimers. Plasmonic dimers (left) only have electric dipoles which couple under a single polarization while dielectric dimers have both electric dipoles and magnetic dipoles that couple under the orthogonal polarizations.

In this study, a nanodimer consisting of two silicon (Si) nanocylinders of diameter 140 nm and height 150 nm placed on a quartz substrate is considered. Experimentally, gaps of 30 nm, 60 nm and 120 nm are tested for varying degrees of coupling between the two particles. The system is studied at visible wavelengths for both X- and Y-polarizations of incident light (using the notation in Figure 1).

Electromagnetic simulations are performed using the Finite Difference Time Domain method (Lumerical FDTD). A silicon dimer is placed on a quartz substrate and illuminated using a linearly polarized plane wave from the far-field, beneath the sample. Material parameters are taken from ellipsometric measurements of amorphous silicon films used in the experiments. Field monitors are used to observe the fields through and around the dimer. The key simulation results for a dimer with a 30nm gap, are illustrated in Figure 2. For X-polarized light, the dimer shows a single scattering peak at a wavelength of 600nm (see Figure 2a). For Y-polarized light, the dimer shows two scattering peaks at 560nm and 650nm (Figure 2d). This is consistent with earlier theoretical studies of far-field scattering spectra of a silicon nanodimer system [17].

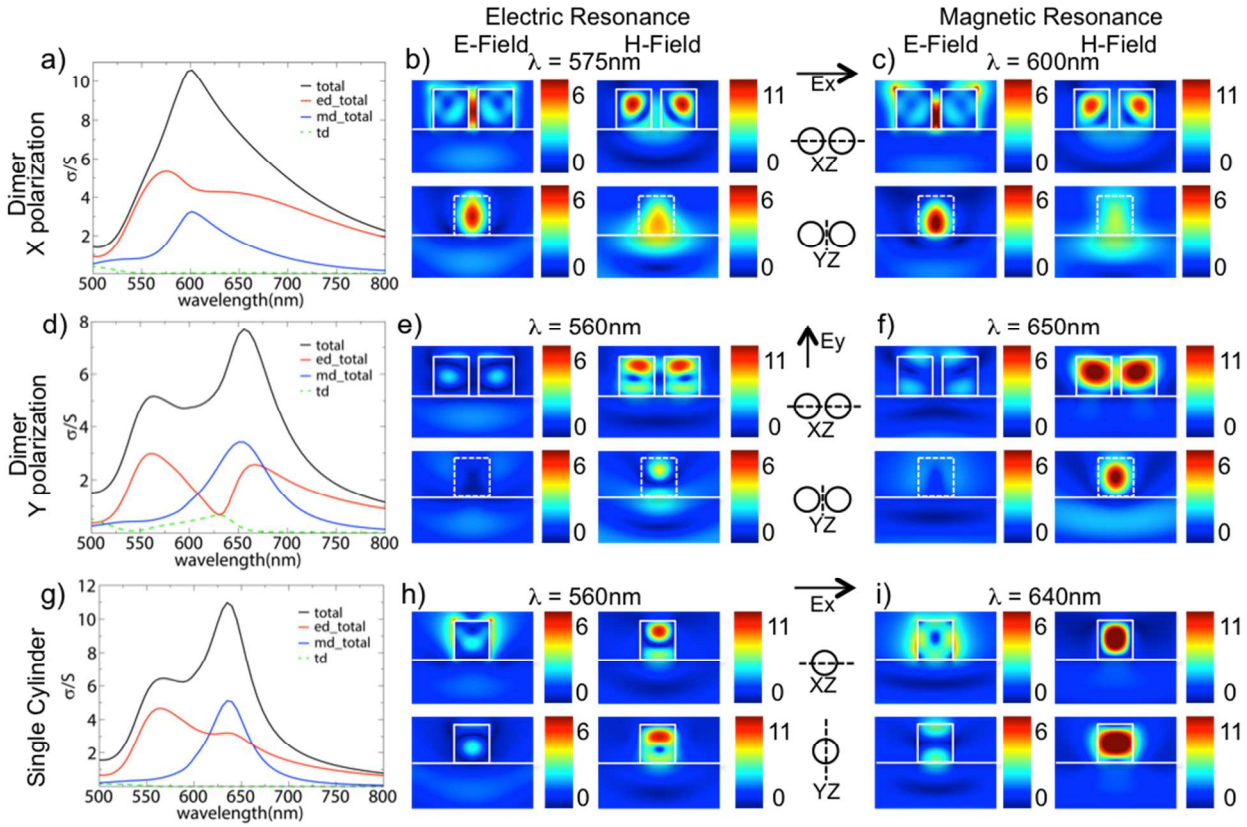

Figure 2. Numerical results for a silicon dimer (a-f) and a single cylinder (g-i) excited by plane wave from the substrate side. Each cylinder has a diameter of 140nm, a height of 150 nm and a gap of 30nm; (a-c) X-Polarized light scattering spectrum with mode decomposition; ed: total electric dipole = Cartesian electric dipole + toroidal dipole, md: magnetic dipole and td: toroidal dipole, plus cross section E- and H- field maps for the electric dipole resonance at 575nm and magnetic dipole resonance at 600nm. (d-f) Same as (a-c) but for Y-Polarized light, the electric dipole resonance is plotted at 560nm and the magnetic dipole resonance at 650nm. (g-i) Same as (a-c) but for the case of a single cylinder, the electric dipole resonance is plotted at 560nm and the magnetic dipole resonance at 640nm. For all maps, both electric and magnetic field amplitudes are normalized to incident plane wave. The size of each map is 450nm x 350nm. White lines indicate the substrate and particle positions.

To gain a deeper insight into the different modes of the system, the mutipole decomposition approach is employed [24, 25]. Due to the presence of the substrate, it is performed by integration of the polarization currents induced within the particles [24]. The multipoles are defined in a Cartesian basis with coordinates' center coinciding with the dimer's center of mass. In addition to conventional electric and magnetic multipole moments this representation includes toroidal moments, the magnetic dipole mean-square radius [26, 27] and fully takes into account substrate interactions while computing equivalent multipoles. For simplicity, when computing the cross-sections associated with each multipole, they are considered to radiate into air (thus, the total cross section is slightly higher than the sum over contributions).

The multipole decomposition for X-polarized light reveals that the single peak in the scattering spectrum is due to an overlap of the dipolar electric and magnetic resonances (Figure 2a). For Y-polarized light, the total scattering cross section has two peaks (Figure 2d) which closely resembles that of a single silicon cylinder (Figure 2g). The multipole decomposition reveals a feature that has not been reported in previous theoretical studies [17], namely, a pronounced dip in the total electric dipole contribution. The dip stems from the interaction between the Cartesian electric dipole moment and the toroidal dipole moment which, due to their similar radiated fields, are able to destructively interfere [26, 27]. The toroidal dipole moment is generated by the magnetic dipoles induced in the disks that point in the same direction but are not fully parallel due to the electric-magnetic dipole interaction. As these features originate from the electric to magnetic dipole interaction, they are a unique to systems with a magnetic dipole and thus not present in metallic dimers (see Supplementary Figure S1 for more details).

The simulated electric and magnetic near-field profiles at resonant wavelengths are also shown in Figure 2. For the dimer with X-polarized light there is spectral overlap of both electric and magnetic field resonances. For the electric field, a hotspot is clearly observed between the two particles (Figures 2b, 2c). Enhancements are observed for the magnetic field as well, but these are mostly confined inside the individual silicon cylinders (Figures 2b, 2c). For the case of Y-polarized light, the 560nm resonance (Figure 2e) is dominated by the individual electric dipoles aligned towards Y-direction while the 650nm (Figure 2f) resonance is dominated by the coupled magnetic dipoles.

It is clearly observed that there is an enhanced and accessible (outside of the particles) magnetic field for both X- and Y-polarized light. In the gap between the particles, the magnetic field has a higher enhancement value for Y-polarized light (over 6x) compared to X-polarized light (~3x). The high enhancement for the Y-polarized case is due to coupling between two aligned magnetic dipoles of the particles. The enhancement inside the gap is lower than that inside the nanoparticles (>10) but still high enough to be accessible for near-field measurements or radiation enhancement of localized emitters. Deeper theoretical analysis of the magnetic field enhancement of the silicon dimer as a function of the gap shows that the magnetic field enhancement in the gap can reach a value of 10 for a gap of 5nm (see Supplementary Figure S3). This value is similar to the magnetic field enhancement inside of each silicon nanoparticle.

The electric field shows strong localization in the gap for the case of X-polarized light (over 6) with smaller localization for the case of Y-polarized light (~4x). For X-polarized light, the electric field enhancement is due to coupling of aligned electric dipole resonances. It can also be affected by discontinuity of the normal component of electric field **E** at high-dielectric contrast interface similar to high-index dielectric slot waveguides [28]. For X-polarized light, the electric

field in the gap is stronger at the magnetic dipole resonance than at the electric dipole resonance. This can be explained by enhanced circular displacement currents of the electric field, which generate the magnetic dipole resonance. At the electric dipole resonance (575 nm) the contribution from the magnetic dipole is low, therefore the observed enhancement is attributed to the electric dipole mode only. In comparison, at the magnetic dipole resonance (600 nm) a superposition of both ED and MD modes is observed, which leads to higher collective enhancement of electric field.

To experimentally observe the discussed field enhancement, dimers of silicon nanoparticles were fabricated using a standard top-down nanofabrication approach. A 150nm thick amorphous silicon (Si) film is grown on a cleaned quartz substrate using inductively couple plasma chemical vapor deposition (Plasmalab System 380, Oxford Instruments). The dielectric function of the fabricated amorphous films is measured through the visible spectral range using ellipsometry. Electron beam lithography (Elionix, 100kV) is performed using Hydrogen silesquioxane (HSQ, Dow Corning, XR-1541-002) as the resist. Unexposed HSQ is removed with Tetramethylammonium hydroxide (TMAH, 25%). The sample is then etched using an inductively coupled plasma etcher (Plasmalab System 100, Oxford) to create Si nanodimers on the quartz substrate. The resultant structures are twin 150nm tall Si nanopillars with a diameter of 140nm. Gaps of 30nm, 60nm and 120nm are explored. The dimers are fabricated with a 5 micron pitch to allow for measurements of single uncoupled dimers.

The near-field profiles are studied experimentally with a Near-Field Scanning Optical Microscope (NSOM, from Nanonics Imaging Ltd). The sample is illuminated from the far-field using linearly polarized light, focused to a spot size of approximately 5 microns on the sample. The light originates from a supercontinuum source (SuperK Power, NKT Photonics) and specific

wavelengths are selected using a variable bandpass filter (SuperK Varia, NKT Photonics) and then polarized with a Glan Thompson prism. Near-field maps are created by collecting light in a transmission configuration through a tapered fiber (coated with Chrome and Gold) with a 110nm aperture. The wavelength is adjusted throughout the visible with a bandwidth of 10nm. To avoid any contribution of polarization sensitivity of the tip, the sample was rotated 90^{o} relative to the incident light polarization to measure the orthogonal polarization. Near-field maps are compiled for X- and Y-polarizations of incident light normalized to an averaged background signal >1 micron apart from the dimers.

Experimental near-field maps are illustrated in Figure 3 for wavelengths throughout the visible for both X- and Y-polarized light (For more in-depth mappings, see Supplementary Figures 4, 5 and 6). These are directly compared with simulations of electromagnetic fields collected by an NSOM tip. To account for the sensitivity of the NSOM probe in the simulations, a method based on the electromagnetic reciprocity theorem [29] is applied (this is similar to Refs. [30, 31]). According to this approach the signal collected by a near-field probe is determined by a specific convolution integral (mutual impedance) of the fields emerging from the aperture of the tip operating in excitation mode with the fields in the vicinity of the structure under study. The simulated near-field images correspond well to the experimental images.

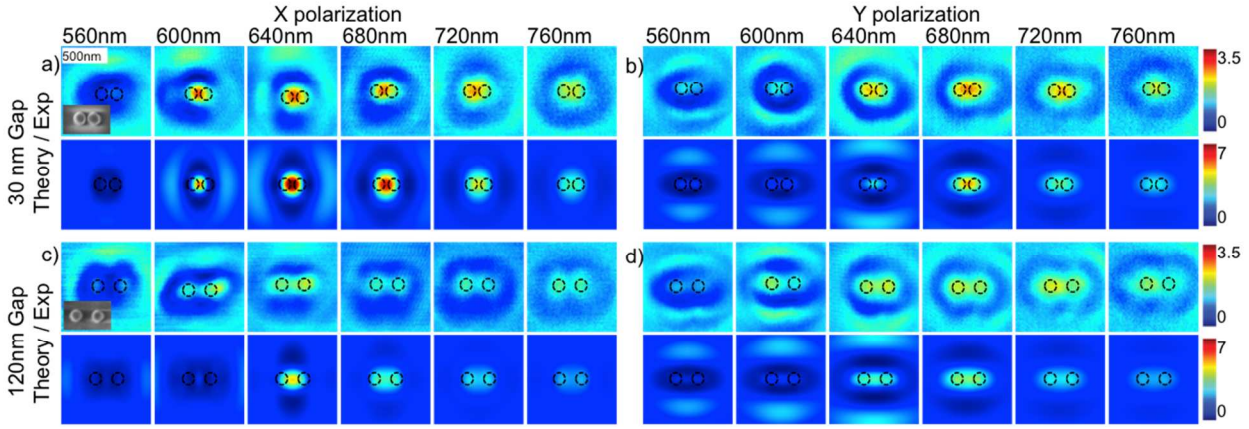

Figure 3. Experimental near-field maps of Si nanodimers compared with simulated near-field maps, as a function of wavelength, dimer gap dimension and polarization. (a) and (b) show the 30nm gap dimer with X- and Y-polarized light respectively. (c) and (d) show 120nm gap dimer with X- and Y-polarized light respectively. Each column represents a different wavelength, labeled at the top. The area of each plot is 1x1μm.

Distinct resonance features and evolution as a function of wavelength are observed for the four gap and polarization cases in figure 3. For the case of the 30nm gap and X-polarized light, the dimer provides a near-field absorptive response at 560nm. This quickly turns into an enhancement effect as the near-field grows to a maximum at 640nm with a circular feature surrounded by near-field extinction. This feature evolves and decreases in intensity through the red. At 760 nm, the map shows an elongated feature with two lobes.

Looking at Y-polarized light for the 30nm gap, the mode starts out, at 560 nm, as a minor elongated feature in the X-direction, surrounded by a null. As the wavelength shifts to the red, an X-elongated feature grows in intensity at the center with a field suppression around it. It reaches a maximum and then decreases, while maintaining its elongated shape as the wavelength moves to red.

For the case of the 120nm gap with X-polarized light, the NSOM features closely resemble that of two separate particles. For 560nm, extinction in the form of two adjacent particles is clearly observed. The near-field feature of each particle increases in intensity and then decreases at longer wavelengths. The case of the 120 nm gap with Y-polarized light, is fairly similar to the X-polarized case, but a slightly higher NSOM signal-enhancement value is measured along with a stronger resonance through the red portion of the spectrum. This is attributed to moderate coupling between the induced magnetic dipoles positioned end to end in the X-direction.

Comparing the NSOM maps obtained for the dimers with 30 and 120 nm gap one can immediately see that for the case of the smaller gap, the NSOM signal reaches larger enhancement for both polarizations. This provides experimental evidence of field localization via electromagnetic coupling of the two silicon nanocylinders.

The collected NSOM signal consists of both electric and magnetic fields. As it can be seen from simulated field components (see Supplementary Figures 3, 4 and 5) the experimentally measured signal strongly resembles that of the transverse magnetic field, Hy for the X-polarization case and Hx for the Y-polarization case, with more minor contributions from the transverse electric fields.

The electromagnetic response of isolated Silicon nanodimers of three different gaps (30nm, 60nm and 120nm) has been experimentally mapped in the near-field throughout the visible portion of the spectrum. A strong spectral response is observed for each of the three gaps for two orthogonal polarizations. The strongest enhancement (3.5) is observed for X-polarized light with the 30nm gap; in this case, there is a coupled resonance response of the electric field and a strong magnetic field response for dimer. The weakest enhancement (2.0) is observed for X-polarized light and the 120nm gap; the electric field and magnetic field response resembles that of two isolated nanoparticles.

From the simulations, it is clear that the highest magnetic fields occur inside the silicon nanoparticles. However, the simulations in conjunction with the near-field experiments clearly show that enhanced magnetic fields are accessible outside of the silicon, both in the gap of the dimer and in the plane above the dimer. These enhancements are available for both X- and Y-polarizations with stronger magnetic fields for the Y-polarized case, where the magnetic dipoles couple with each other.

In conclusion, we have presented, for the first time to our knowledge, the experimental evidence of near-field enhancement of the magnetic fields with silicon resonant nanodimers at visible frequencies. The response of the system has been studied as a function of wavelength, polarization and gap. Theory and numerical simulations predict that such a structure should have a strong magnetic response; and our simulations confirm a very good correlation with the near-field measurements. When the simulated near-fields are broken down into their components, it is confirmed that the resonance measured in the near-field is strongly magnetic in nature, for both X- and Y-polarizations. Additionally, we have conducted a complete analysis of the modes excited inside the dielectric nanodimer system by means of the multipole decomposition. This analysis has revealed excitation of a toroidal dipole moment which interferes with the Cartesian electric dipole moment resulting in a dip in the total electric dipole radiation. This is the first reporting of toroidal dipole excitation in dielectric nanodimer antennas. The dimer system is the basic building block for many nanophotonics systems. The results demonstrated in this paper lay the ground work for future engineering of the magnetic field response at optical frequencies with high-index dielectric nanostructures for the ultimate control on the subwavelength scale.

Author Contributions

RMB performed the near-field experiments and analysis, and wrote the manuscript with inputs from all coauthors. DP performed simulation of near-field detected by the NSOM tip and contributed to NSOM data acquisition and analysis. YFY performed nanofabrication of the silicon dimers. DM performed FDTD simulation of far- and near-field properties of the silicon dimers. RPD performed the multipole decomposition calculations and analysis. LG developed and performed the Si etching for the sample. AKS contributed to NSOM data acquisition and

analysis, and coordinated the simulation work. YSK supervised the work of ITMO team. BL supervised the work of DSI team. AIK proposed the initial idea, organized and coordinated the whole work. All authors contributed to the manuscript preparation and reviewed the final version of the manuscript.

Funding Sources

The authors at DSI were supported by DSI core funds. The work at IMTO University was financially supported by Government of Russian Federation (projects 14.584.21.0009 10, Zadanie no. 3.561.2014/K, 074-U01) and Russian Foundation for Basic Research.

Notes

The authors declare no competing financial interests.

ACKNOWLEDGMENT

Fabrication, Scanning Electron Microscope Imaging and NSOM works were carried out in facilities provided by SnFPC@DSI (SERC Grant 092 160 0139). Yang Yi and Vytautas Valuckas are acknowledged for SEM work at DSI. Yi Zhou (DSI) is acknowledged for silicon film growth. Yeow Teck Toh (DSI) and Doris Ng (DSI) are acknowledged for development of the silicon nanofabrication procedure. Ivan Sinev (ITMO University) is acknowledged for assistance in modeling of the NSOM probe sensitivity.

REFERENCES

1. Evlyukhin, A. B.; Reinhardt, C.; Seidel, A.; Luk'yanchuk, B. S.; Chichkov, B. N. Optical response features of Si-nanoparticle arrays. *Phys. Rev. B* **2010**, *82*, 045404.

2. García-Etxarri, A.; Gómez-Medina, R.; Froufe-Pérez, L. S.; López, C,; Chantada, L.; Scheffold, F.; Aizpurua J.; Nieto-Vesperinas, M.; Sáenz, J. J. Strong magnetic response of submicron silicon particles in the infrared. *Opt. Express* **2010**, *19*, 4815-4826.

3. Krasnok, A. E,; Miroshnichenko, A. E,; Belov, P. A.; Kivshar, Y. S. All-Dielectric Optical Nanoantennas. *Opt. Express* **2012,** *20*, 20599-20604.

4. Miroshnichenko, A. E.; Luk'yanchuk, B.; Maier, S. A.; Kivshar, Y. S. Optically Induced Interaction of Magnetic Moments in Hybrid Metamaterials. *ACS Nano* **2012**, *6***,** 837-842.

5. Schmidt, M. K.; Esteban, R.; Sáenz, J.; Suárez-Lacalle, I.; Mackowski, S.; Aizpurua, J. (2012). Dielectric antennas-a suitable platform for controlling magnetic dipolar emission. *Opt. Express* **2012**, *20*, 13636-13650.

6. Ginn, J. C.; Brener, I.; Peters, D. W.; Wendt, J. R.; Stevens, J. O.; Hines, P. F.; Basilio, L. I.; Warne, L. K.; Ihlefeld, J. F. Clem, P. G.; Sinclair, M. B. Realizing optical magnetism from dielectric metamaterials. *Phys. Rev. Lett.* **2012**, *108*, 097402.

7. Kuznetsov, A. I.; Miroshnichenko, A. E.; Fu, Y. H.; Zhang, J. B.; Luk'yanchuk, B. Magnetic light. *Sci. Rep.* **2012**, *2*, 492 (1-6).

8. Evlyukhin, A. B.; Novikov, S. M.; Zywietz, U.; Eriksen, R. L.; Reinhardt, C.; Bozhevolnyi, S. I.; Chichkov, B. N. (Demonstration of magnetic dipole resonances of dielectric nanospheres in the visible region. *Nano Lett.* **2012**, *12*, 3749-3755.

9. Fu, Y. H.; Kuznetsov, A. I.; Miroshnichenko, A. E.; Yu, Y. F.; Luk'yanchuk, B. Directional visible light scattering by silicon nanoparticles. *Nat. Commun.* **2013**, *4*, 1527 (1-6).

10. Person, S.; Jain, M.; Lapin, Z.; Sáenz, J. J.; Wicks, G.; Novotny, L. Demonstration of zero optical backscattering from single nanoparticles. *Nano Lett.* **2013**, *13*, 1806-1809.

11. Krasnok, A. E.; Belov, P. A.; Miroshnichenko, A. E.; Kuznetsov, A. I.; Luk'yanchuk, B. S.; , Kivshar, Y.S. All-dielectric optical nanoantennas, In *Progress in Compact Antennas* Huitema, L., Eds.; *InTech* 2014*;* pp. 143-172.

12. Staude, I.; Miroshnichenko, A. E.; Decker, M.; Fofang, N. T.; Liu, S.; Gonzales, E.; Dominguez J.; Luk, T.S.; Neshev, D.N.; Brener, I,; Kivshar, Y. Tailoring directional scattering through magnetic and electric resonances in subwavelength silicon nanodisks. *ACS Nano* **2013**, *7*, 7824-7832.

13. Moitra, P.; Yang, Y.; Anderson, Z.; Kravchenko, I. I.; Briggs, D. P.; Valentine, J. Realization of an all-dielectric zero-index optical metamaterial. *Nat. Photon.* **2013**, *7*, 791-795.

14. Liu, S.; Sinclair, M. B.; Mahony, T. S.; Jun, Y. C.; Campione, S.; Ginn, J.; Bender, D.A.; Wendt, J.R.; Ihlefeld, J. F.; Clem, P.G.; Wright, J.B.; Optical magnetic mirrors without metals, *Optica* **2014**, *1*, 250-256.

15. Wu, C.; Arju, N.; Kelp, G.; Fan, J. A.; Dominguez, J.; Gonzales, E.; Tutuc, E.; Brener, I.; Shvets, G. Spectrally selective chiral silicon metasurfaces based on infrared Fano resonances. *Nat. Commun.* **2014**, *5*, 3892 (1-9).

16. Decker, M.; Staude, I.; Falkner, M.; Dominguez, J.; Neshev, D. N.; Brener, I.; Pertsch, T.; Kivshar, Y. S. High efficiency dielectric Huygens‘ surfaces. *Adv. Opt. Mater.* **2015**, DOI: 10.1002/adom.201400584

17. Albella, P.; Poyli, M. A.; Schmidt, M. K.; Maier, S. A.; Moreno, F.; Sáenz, J. J.; Aizpurua, J. Low-loss Electric and Magnetic Field-Enhanced Spectroscopy with subwavelength silicon dimers. *J. Phys. Chem. C* **2013**, *117*, 13573-13584.

18. Miroshnichenko, A. E.; Kivshar, Y. S. Fano resonances in all-dielectric oligomers. *Nano Lett.* **2012**, *12* , 6459-6463.

19. Chong, K. E.; Hopkins, B.; Staude, I.; Miroshnichenko, A. E.; Dominguez, J.; Decker, M.; Neshev, D. N.; Brener, I.; Kivshar, Y. S. Observation of Fano Resonances in All-Dielectric Nanoparticle Oligomers. *Small* **2014**, *10*, 1985-1990.

20. Sigalas, M. M.; Fattal, D. A.; Williams, R. S.; Wang, S. Y.; Beausoleil, R. G. Electric field enhancement between two Si microdisks. *Opt. Express* **2007**, *15*, 14711-14716.

21. Albella, P.; Alcaraz de la Osa, R.; Moreno, F.; Maier, S. A. Electric and magnetic field enhancement with ultra-low heat radiation dielectric nanoantennas: Considerations for surface enhanced spectroscopies. *ACS Photon.* **2014**, *1*, 524-529.

22. Wang, C.; Jia, Z. Y.; Zhang, K.; Zhou, Y.; Fan, R. H.; Xiong, X.; Peng, R. W. Broadband optical scattering in coupled silicon nanocylinders. *J. Appl. Phys.* **2014**, *115*, 244312.

23. Boudarham, G.; Abdeddaim, R.; Bonod, N. Enhancing the magnetic field intensity with a dielectric gap antenna. *Appl. Phys. Lett.* **2014**, *104*, 021117.

24. Grahn, P.; Shevchenko, A.; Kaivola, M. Electromagnetic multipole theory for optical nanomaterials. *New J. Phys.* **2012**, *14*, 093033.

25. Chen, J.; Ng, J.; Lin, Z.; Chan, C. T. Optical pulling force. *Nat. Photon.* **2011**, *5*, 531-534.

26. Fedotov, V. A.; Rogacheva, A. V.; Savinov, V.; Tsai, D. P.; Zheludev, N. I. Resonant Transparency and Non-Trivial Non-Radiating Excitations in Toroidal Metamaterials. *Sci. Rep.* **2013**, *3*, 2967 (1-5).

27. Miroshnichenko, A. E.; Evlyukhin, A. B.; Yu, Y. F.; Bakker, R. M.; Chipouline, A.; Kuznetsov, A. I.; Luk'yanchuk, B.; Chichkov, B. N.; Kivshar, Y. S. Seeing the unseen: observation of an anapole with dielectric nanoparticles. *ArXiv:1412.0299* (**2014)**.

28. Almeida, V. R.; Xu, Q.; Barrios, C. A.; Lipson, M. Guiding and confining light in void nanostructure. *Opt. Lett.* **2004**, *29*, 1209-1211.

29. Sinev, I. S.; Voroshilov, P. M.; Mukhin, I. S.; Denisyuk, A. I.; Guzhva, M. E.; Samusev, A. K.; Belov, P.; Simovski, C. R. Demonstration of unusual nanoantenna array modes through direct reconstruction of the near-field signal. *Nanoscale* **2015**, *7*, 765-770.

30. Porto, J. A.; Carminati, R.; Greffet, J. J. Theory of electromagnetic field imaging and spectroscopy in scanning near-field optical microscopy. *J. Appl. Phys.* **2000**, *88*, 4845-4850.

31. Le Feber, B.; Rotenberg, N.; Beggs, D. M.; Kuipers, L. Simultaneous measurement of nanoscale electric and magnetic optical fields. *Nat. Photon.* **2014**, *8*, 43-46.

Table of Contents Graphic